Investigation of Self-Starting Capability of Vertical Axis Wind Turbines Using a Computational Fluid Dynamics Approach

Alexandrina Untaroiu[1]
e-mail: au6d@virginia.edu

Houston G. Wood

Paul E. Allaire

Robert J. Ribando

Rotating Machinery and Controls (ROMAC) Laboratory,
University of Virginia,
Mechanical and Aerospace Engineering Department,
122 Engineer's Way,
Charlottesville, VA 22904-4746

Vertical axis wind turbines have always been a controversial technology; claims regarding their benefits and drawbacks have been debated since the initial patent in 1931. Despite this contention, very little systematic vertical axis wind turbine research has been accomplished. Experimental assessments remain prohibitively expensive, while analytical analyses are limited by the complexity of the system. Numerical methods can address both concerns, but inadequate computing power hampered this field. Instead, approximating models were developed which provided some basis for study; but all these exhibited high error margins when compared with actual turbine performance data and were only useful in some operating regimes. Modern computers are capable of more accurate computational fluid dynamics analysis, but most research has focused on horizontal axis configurations or modeling of single blades rather than full geometries. In order to address this research gap, a systematic review of vertical axis wind-power turbine (VAWT) was undertaken, starting with establishment of a methodology for vertical axis wind turbine simulation that is presented in this paper. Replicating the experimental prototype, both 2D and 3D models of a three-bladed vertical axis wind turbine were generated. Full transient computational fluid dynamics (CFD) simulations using mesh deformation capability available in ANSYS-CFX *were run from turbine start-up to operating speed and compared with the experimental data in order to validate the technique. A circular inner domain, containing the blades and the rotor, was allowed to undergo mesh deformation with a rotational velocity that varied with torque generated by the incoming wind. Results have demonstrated that a transient CFD simulation using a two-dimensional computational model can accurately predict vertical axis wind turbine operating speed within 12% error, with the caveat that intermediate turbine performance is not accurately captured.* [DOI: 10.1115/1.4004705]

Keywords: wind turbine, self-starting, CFD, computational methods, design tool

1 Introduction

The windmill has long been a basic tool for harnessing natural power, from the Persian cloth-sail mills of the 9th century to the classic Dutch mills seen in medieval Europe [1]. This latter configuration, the horizontal axis wind turbine (HAWT) was and continues to be the most popular for large-scale power production; however, the VAWT type has been revisited repeatedly for several reasons. In particular, the Darrieus-patented H-type rotor is attractive for its ease of maintenance, ability to use a direct-drive generator, independence on yaw, decreased noise of operation, simplicity of blade manufacture, and decreased incidence of wildlife collisions due to visibility and lower operating speed [2–5].

In spite of these features, VAWTs have lagged considerably in development and implementation compared to their HAWT counterparts. Much of this disparity is due to field experience from the 1970s and 1980s. At this time, a number of egg-beater or troposkien-style VAWTs were built and tested in comparison with 2 and 3-bladed fan type HAWTs for power production in the megawatt range [6–8]. Many of these turbines proved incapable of efficiencies comparable to the HAWT at such high power ratings. Moreover, some of those with symmetric airfoils demonstrated an inability to escape the negative torque or "start-up" band of operating speeds. They were thus deemed a dead-end in the popular view, despite recommended solutions by researchers such as Baker [9]. As a result of this experience, the commercial wind turbine industry largely focused on massive HAWTs, which have become standard in power production.

2 CFD Modeling and Wind Turbines

2.1 HAWT. As with seemingly all aspects of wind turbine research, CFD simulations are easier with HAWTs than VAWTs. Particularly in the last decade, a number of Navier–Stokes predictions have been published in conjunction with NREL Phase VI rotor, an experimental HAWT examined in detail at the National Aeronautics and Space Administration, NASA Ames wind tunnel [10–13]. These studies demonstrate several reduction techniques; one of the most useful is the modeling of only one blade, which can be done because an HAWT blade will not encounter severe wake interference from other blades as is the case for VAWTs.

2.2 VAWT. In the meantime, the numerical community continued to examine alternative configurations for VAWTs, recognizing that the experimental work had only addressed a small subset of potential designs. Early numerical studies were hampered by limited computer processing ability, and utilized

[1]Corresponding author.

Contributed by the Solar Energy Division of ASME for publication in the JOURNAL OF SOLAR ENERGY ENGINEERING. Manuscript received October 15, 2010; final manuscript received July 20, 2011; published online October 13, 2011. Assoc. Editor: Spyros Voutsinas.

high-end approximations such as the Paraschivoiu double-multiple streamtube model, vortex method, local-circulation model or modified cascade theory [14–18]. Some common example codes include variations on CARDAA and VDART [19,20]. Each has its strengths and weaknesses, and provides the majority of the foundation for modern parametric studies on the subject. Such studies have only had success in replicating portions of VAWT performance with significant error (the exact values depend on operating speed, but errors of 25% are not unusual).

Particularly in the realm of self-starting, Hill et al. [21] note the shortcomings of numerical modeling: "while the researchers' physical turbine can be made to reliably self-start in wind tunnel conditions, reaching full design tip-speed ratio (TSR), their computer model remains at a much lower speed plateau indefinitely". This is characteristic of prior numerical methods, whose approximations lead to accuracy only in restricted realms of operation. In this case, it was observed that turbine performance in the plateau region was necessarily sensitive to changes in the Reynolds number; that is, in order for velocity to be approximately constant, the positive and negative torques experienced by the turbine must be nearly equal, and the eventual acceleration from plateau must represent a very small net positive. Because the researchers were limited to lift and drag information at discrete angles of attack dictated by previous experimental studies, it was hypothesized that their sample rate was not high enough to capture development of this slight positive torque.

CFD can be tuned to operate at as small a timestep as the researcher desires, theoretically overcoming the problem posed above – force and torque information come directly from the simulation at the sample rate specified. In spite of this, very little of the previously published research examining the effects of chord length, solidity, airfoil shape, tip-speed ratio, pitching, etc. has been replicated or combined into an intensive CFD study, although small VAWTs continue to be produced and marketed. In order for these technologies to be effective in utilizing the advantages of VAWTs, such research must be undertaken.

One example of this is the recently published work of Howell et al. [22], which compares 2D, 3D and experimental wind tunnel models using the NACA0022 airfoil. The researchers tested a small VAWT at realistic wind speeds in the Sheffield University's low speed wind tunnel, varying wind speed, TSR, solidity and blade surface finish. This experimental data was then compared with both a 2D and 3D CFD simulation using Fluent (ANSYS Inc., Cannonsburg, PA) in order to examine accuracy and visualize the flow structures around the turbine. In this case, the turbine was not allowed to ramp up from a stop to its natural operating speed. Instead, a torque brake was applied at discrete points to determine the coefficient of performance (C_p) at various TSR. This methodology was replicated in simulation, wherein the TSR was fixed and the ensuing instantaneous torque was plotted over a number of cycles. The average value was used to calculate performance. Comparing the C_p versus TSR graphs at increasing incoming wind velocities, it can be seen that the 2D simulation consistently overpredicts performance, while the 3D simulation generally underpredicts it, but is within the computed experimental error (a quite high 20%). Both appear to give worse predictions at higher TSR (although the data only range from 1.8 to 2.85, which is very low for VAWTs). The authors postulate that the discrepancy in 2D and 3D data results from failure to capture tip vortex shedding; this phenomenon is well documented by flow visualization elsewhere [23].

In order to examine the general applicability of this finding, as well as determine whether CFD would support prior numerical and experimental conclusions regarding VAWT design, the Rotating Machinery and Controls laboratory of the University of Virginia (ROMAC) set out to perform parametric studies using CFX (ANSYS Inc., Cannonsburg, PA). Due to the scope of this work, the studies were divided into validation and variation of parameters, with both 2D and 3D models considered. This paper will address the initial methodology, which is instructive for future work; before any further studies can be done, it must be demonstrated that full CFD can overcome the plateau problem highlighted by Hill et al. [21] with better accuracy than that reported by Howell et al. [22] and discussed above.

3 Methods

Unlike many similar studies, the aforementioned experimental data published by Hill et al. [21] encompasses a much longer timeframe—the data extends over almost 200 s taken at a frame rate of 10 Hz, and reports TSR from start-up to operating speed. This is extremely appealing as a validation case, as it allows direct comparison of real behavior rather than a calculated coefficient. Finally, the turbine was tested at a realistic incoming wind speed (6 m/s) rather than the often inflated numbers reported by commercial ventures (15–25 m/s). Thus, the Durham turbine [21] was selected as a good candidate for simulation in this work. This allowed for comparison not only of the initial machinery behavior but also subsequent performance as the turbine ramped up to full operating speed. As was noted before, many simpler approximations have been successfully utilized for simulation of specific steady-state regimes; the potential benefit of a more computationally intensive CFD approach is to encapsulate behavior over *all* regimes, including any hysteresis effects.

The setup for the aforementioned experiment is detailed in Hill et al. [21]. To summarize, the straight-rotor turbine utilized three blades of profile NACA0018 with a chord length of 0.083 m, a swept radius of 0.375 m, a height of 0.6 m, and a moment of inertia of 0.018 kg/m^2. These were mounted such that the bottom of each blade was 0.26 m from the ground and the center coincided with that of the wind tunnel working section.

The turbine axis of rotation was 1.5 m downstream of the entry to the working section, which had an inlet wind speed of 6 m/s. The whole was enclosed in a plenum of 3.3×2.15 m. This setup is summarized in Fig. 1.

3.1 Model Geometry and Mesh Generation. The simulated region was divided into two domains, a circular inner domain and a rectangular outer domain, respectively. The inner domain contained all of the turbine components, while outer domain modeled the inlet, outlet, and side shear layers of the tunnel. Both 2D and 3D computational models were generated. The number of grid elements for each numerical model (Table 2) was selected based on a grid convergence study performed to ensure the optimal trade-off between computational time and the accuracy of the solution. For the 3D CFD simulations, a Solidworks model of the whole turbine and jet region was generated and subsequently meshed using ANSYS-meshing built-in capabilities; whereas the 2D model represented a slice of the turbine normal to the axis of rotation along a section of the turbine not containing struts or guide wires (Figs 2–5). Table 2 lists the regional mesh densities and resulting Y_+ values for each computational model.

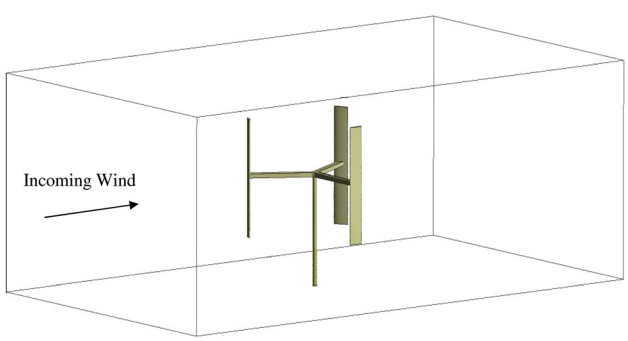

Fig. 1 Durham wind tunnel setup and test prototype

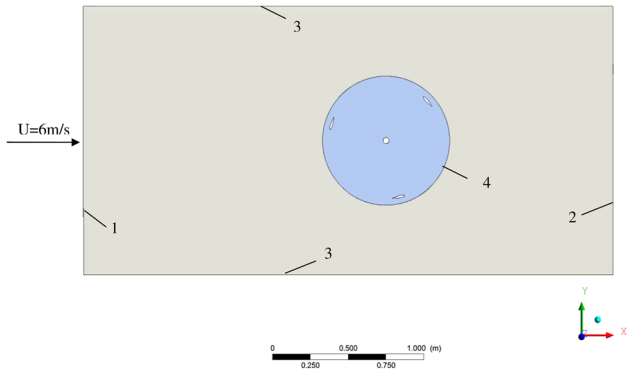

Fig. 2 2D Boundary conditions setup illustrating the inner and outer domain, both set as stationary; (1) inlet, (2) outlet, (3) no-slip adiabatic wall, and (4) transient rotor-stator interface

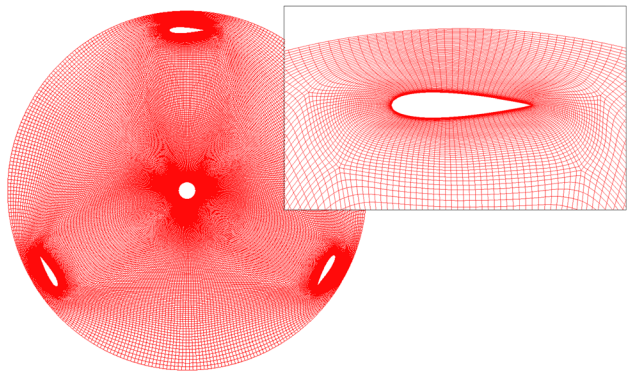

Fig. 3 Structured two dimensional mesh for the Durham wind tunnel; inner domain and detail view of mesh clustered on the blade surface

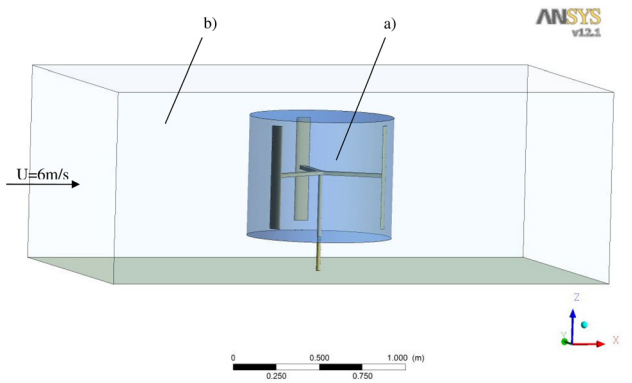

Fig. 4 3D CFD simulation setup illustrating (*a*) the inner domain undergoing mesh deformation and (*b*) outer domain

3.2 Boundary Conditions. In this study, the 2D and 3D transient CFD simulation were performed using ANSYS-CFX v12.0. Both inner and outer domains were specified as stationary domains connected by an interface that guaranteed conservation of mass between the two. The circular domain contained the blades as well as a rotor or hub; a subdomain of this was allowed to undergo mesh deformation with a rotational velocity that varied with torque generated by the incoming wind (Fig. 4). This was done in order to ensure a rectilinear wind profile in the approach to the turbine while still capturing the rotation at the blades; the computational load of the simulation was thereby decreased as well.

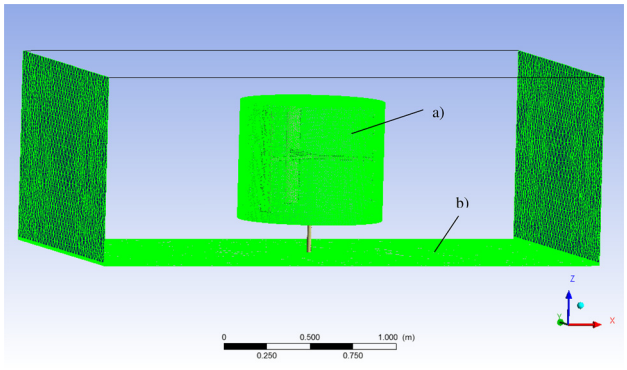

Fig. 5 Unstructured hybrid mesh replicating Durham wind tunnel and VAWT prototype; (*a*) inner domain and (*b*) outer domain

Table 1 Durham vertical axis wind turbine—model parameters

Airfoil	NACA0018
c (m)	0.083
s (m)	0.6
R (m)	0.375
J (kg × m^2)	0.018
J_{eff} (kg × m^2)	0.0012
U (m/s)	6

The subdomain mesh motion was specified with the ANSYS programming language CEL, a byte code compiled language, as follows:

$$r = \sqrt{x^2 + y^2} \tag{1}$$

$$\theta = \arctan(y/x) \tag{2}$$

$$\dot{\theta} = \left(\sqrt{\dot{x}^2_{\text{subdomain}} + \dot{y}^2_{\text{subdomain}}}\right) \Big/ \max\left(r, 10^{-8}\right) \tag{3}$$

$$\ddot{\theta}^n = T_z/\text{Jeff} \tag{4}$$

$$\dot{\theta}^n = \dot{\theta} + \ddot{\theta}^n \cdot t \tag{5}$$

$$\theta^n = \theta + \dot{\theta}^n \cdot t \tag{6}$$

$$x^n = r \cdot \cos(\theta^n) \tag{7}$$

$$y^n = r \cdot \sin(\theta^n) \tag{8}$$

where torque T_z, subdomain velocities $\dot{x}_{\text{subdomain}}$ and $\dot{y}_{\text{subdomain}}$ are retrieved from the simulation, effective moment of inertia J_{eff} is calculated as moment of inertia per unit height, and t is the specified timestep (in the 3D case, J_{eff} is replaced by total J as given in Table 1). The limiter in the denominator of the old angular velocity Eq. (3) is used to avoid a divide-by-zero error at the origin. It may be noted that the discretization of the new value equations appears inconsistent with respect to the iteration index. This is because the positions and velocities are initialized before the simulation runs, while the torque and subdomain velocities are retrieved values that are not calculated until after the first iteration. A more robust finite difference of the old and new values is unavailable since CFX cannot retrieve information from previous iterations. This is an artifact of the program storage process and is unavoidable.

The wind velocity was specified at the inlet as 6 m/s. The sides of the rectangular domain were designated as no-slip walls, while the side opposite the inlet was designated an outlet at atmospheric pressure. The k-e turbulence model, as well as a scalable turbulent wall function, was selected for each CFD simulation. It is a two equation model, which means; it includes two extra transport equations to represent the turbulent properties of the flow, and has

Table 2 CFD models-regional mesh density

	Number of grid elements	
	2D Model ($Y_+ = 1.7$)	3D Model ($Y_+ = 6.3$)
Inner domain	96 k	4.6×10^6
Outer domain	40 k	3.3×10^6
Total	136 k	7.9×10^6

been shown to be useful for flows with relatively small pressure gradients [24].

3.3 Simulation Parameters. In addition to the basic geometric boundary conditions, a vast number of other parameters can be altered in CFD. Because of the large range of length and timescales, an appropriate timestep was unknown *a priori*; the timestep automatically calculated by CFX was used as a guideline and then varied to test for sensitivity. Timesteps of 0.001 and 0.00005 s were examined.

Given the nature of the flow, it was expected that separation effects would impact the turbine performance in some speed regimes. Since VAWTs vary so widely over all parameters within one cycle, and even more so in a full ramp-up, the extent to which accurate separation modeling would affect the overall simulation was unknown. The least computationally intensive approach was therefore selected for initial turbulence testing; this was a standard k-ε turbulence model with scalable wall effects. The turbulence intensity, I, is defined as the ratio of the root-mean-square of the velocity fluctuations, u', to the mean free stream velocity, u. For external flows the value of turbulent intensity at the freestream can be as low as 0.05% depending on the flow characteristics, whereas for internal flows the value of turbulence intensity can be fairly high with values ranging from 1% to 10% being appropriate at the inlet. Based on the experimental setup it was unknown whether a medium (5%) or low (1%) intensity and eddy viscosity ratio at the inlet would be more realistic (or, indeed, whether any measurable difference would be noted). As such, both settings were examined. The turbulence numerics were solved using a first order finite differencing, while the advection utilized a high resolution scheme. The timestepping was accomplished with a second order backward Euler scheme.

Once an appropriate combination of parameters was established, the 2D simulation was allowed to run until a plateau in angular velocity was observed. This combination was repeated for the 3D case in order to determine whether significant differences were present.

4 CFD Results and Comparison With Experimental Data

4.1 Timestep Sensitivity Study. As discussed above, a 2D transient simulation of the Durham VAWT using the k-ε turbulence model with 5% turbulence intensity and eddy viscosity ratio at the inlet was run for several seconds with timesteps of 0.001 and 0.00005 s to determine whether the smaller timestep was necessary. A comparison of angular velocity versus time for both timesteps is shown in Fig. 6.

It can be seen that there is only a slight variation between the two cases, with overall trends being identical. The case using 0.001 s timestep was therefore allowed to run until a steady operating speed plateau was observed.

4.2 Inlet Turbulence Intensity Sensitivity Study. The 2D transient simulation with k-ε turbulence model and a timesptep of 0.001 s was allowed to ramp up from a stop to full operating speed. Cases using both low and medium turbulence intensity and eddy viscosity ratio at the inlet were run to determine whether

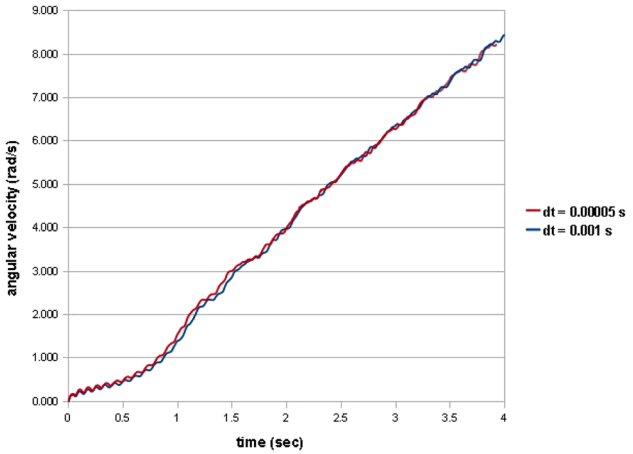

Fig. 6 2D Simulation, angular velocity versus time comparison for two timesteps

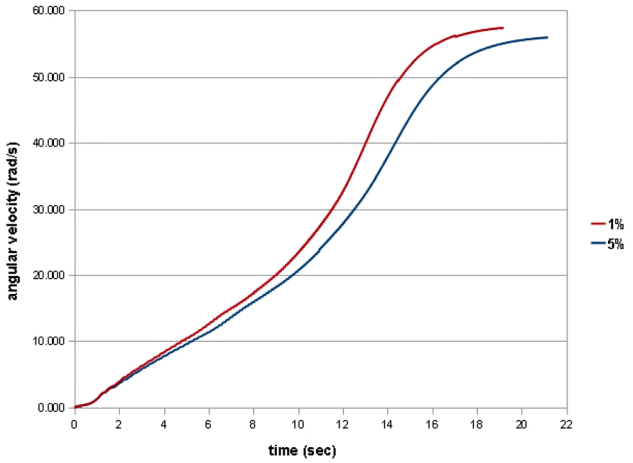

Fig. 7 2D Simulation, angular velocity versus time comparison for two inlet *k-ε* turbulence levels

there were significant differences. A comparison of angular velocity versus time for both cases is shown in Fig. 7.

Taking the ratio of the velocities, it can be seen that the low (1%) inlet turbulence results in an approximately 9% faster turbine rotation on average than the medium inlet turbulence (Fig. 8). This difference drops to approximately 4% at operating speed.

The published Durham turbine experimental data has been converted from TSR to angular velocity $\dot{\theta}$ using Eq. (9).

$$\dot{\theta} = \mathrm{TSR} \cdot \frac{U}{R} \tag{9}$$

The resulting angular velocity is plotted against time along with the 2D k-ε turbulence model simulations in Fig. 9.

Several observations can be made. First, the simulations accelerate to their operating speeds approximately 10 times faster than those experimentally measured. Scaling the simulation time-axis in order to better compare the sets, it can be seen that the medium intensity model accurately predicts the operating speed within about 12% error. Although the experimental uncertainty is not reported for the Durham turbine, other publications have reported up to 20% uncertainty [22]. A more modest 10% error margin is shown below (Fig. 10).

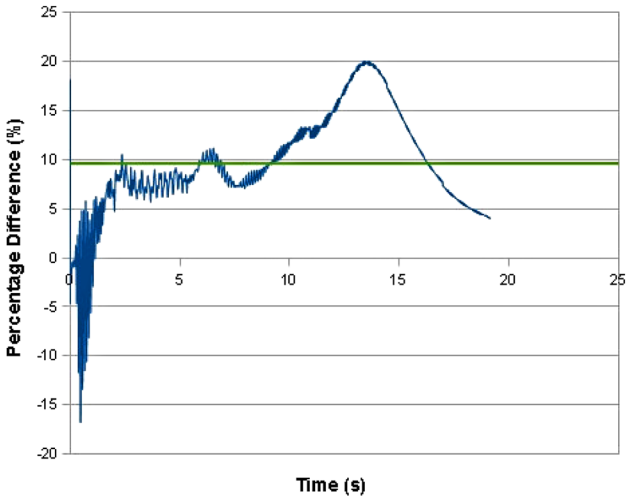

Fig. 8 2D Simulation, percent difference between 1% and 5% level k-ε turbulence models

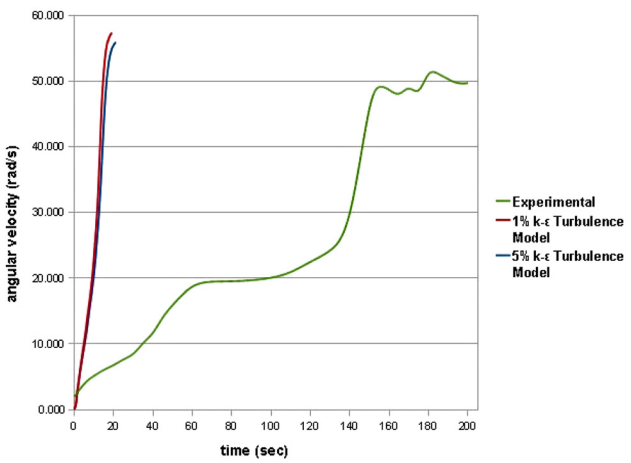

Fig. 9 Comparison of raw 2D *k-ε* simulations with experimental data

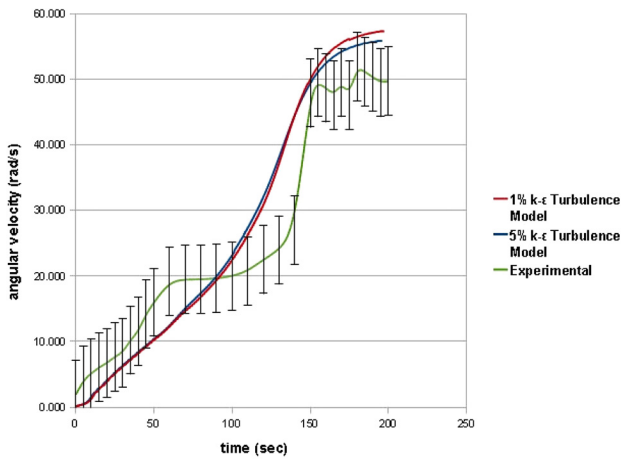

Fig. 10 Comparison of scaled 2D k-ε simulations with experimental data

It should be noted that while the operating speed plateau is fairly realistic, the initial plateau relevant to self-starting phenomena is completely absent in the simulation.

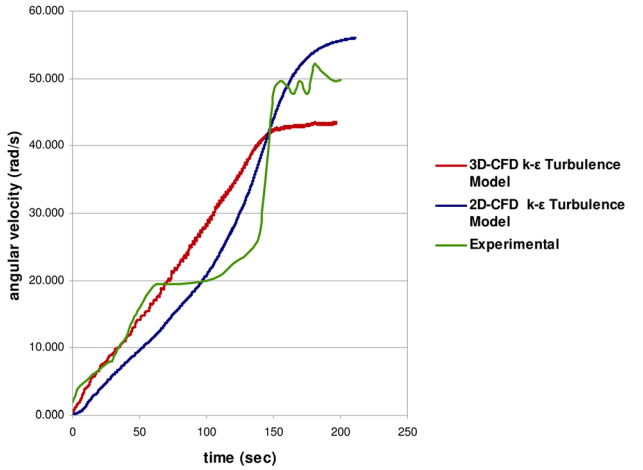

Fig. 11 Comparison of scaled 2D and 3D k-ε simulations with experimental data

4.3 Comparison of 3D Model and Experiment. A 3D transient simulation was run with a timestep of 0.001 s under conditions of medium turbulence intensity and eddy viscosity ratio at the inlet. As illustrated in Fig. 11, the results were compared with both the 2D simulation and the experimental data. It can be seen that the 3D model underpredicts the operating speed, yielding an error of approximately 15%.

5 Discussion

It is observed that both the 2D and 3D simulations using a standard k-ε turbulence model fail to predict an initial velocity plateau prior to the full operating speed. Moreover, both are seen to accelerate over 10 times faster than experimentally measured VAWTs. Logically, the two are linked – because the turbine experiences no period of equilibrium operation before the operating speed is reached, the simulated time is greatly decreased. This does not account for the over-rapid acceleration in the initial linear region or that after the initial plateau point. This discrepancy suggests that some additional source of negative torque is being neglected throughout the simulation – that is, some force in the negative tangential direction. As can be seen in Eq. (4), only the aerodynamic torque was modeled in CFD. The friction effects should have been included, but no data were available to guide the selection of this parameter [21]. It should be noted that, due to the complex variation of angle of attack with position, this force cannot strictly be equated with drag; however, it seems likely that viscous drag is the predominate culprit. It is well-documented that a k-ω model yields better near-wall treatment than the k-ε model, and so this conclusion is not surprising.

In spite of this poor wall treatment, the 2D k-ε model provides a remarkably accurate prediction of the turbine operating speed. To put the reported 12% error in context, at TSR = 3 CARDAAX is shown to yield 15.6% overprediction of Cp, CARDAAV yields 22.7% overprediction, and VDART3 yields 17.8% overprediction for a larger VAWT [14]. Moreover, these models only give hypothetical operational curves of C_p at specified TSR. They do not provide any sort of prediction as to where along this curve the turbine will actually settle. Conversely, the reported full transient 2D CFD simulation allows for predictive examination of the actual turbine behavior in a given wind. Using the k-ε model appears to yield an averaged report of this behavior which needs only a slight correction.

Two issues, then, remain: explanation of the 3D versus 2D results and the failure to predict the initial velocity plateau. Underprediction of operating performance in 3D is consistent with the CFD study reported by Howell et al. [22]. The authors hypothesized that generation of tip vortices which do not appear

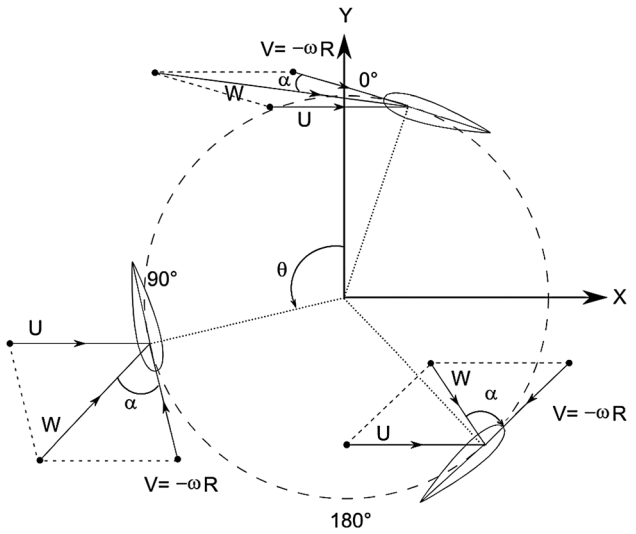

Fig. 12 Velocity vectors on a VAWT Blade for various azimuthal positions

in 2D slowed the turbine considerably. Since vortices obviously *are* shed in reality, however, it is unclear why this would result in lower-than-correct prediction. Additionally, the key to the missing initial velocity plateau may affect the 3D model performance. Returning to the physics of the problem, it is observed that a constant angular velocity implies no angular acceleration, and therefore no torque. Since this is not the case, as a wind turbine would be useless if it generated *no* torque, the prior statement must be amended: the angular velocity is actually constant in average over a cycle, indicating that the angular acceleration *on average* is 0, and the positive and negative torques experienced over the cycle exactly cancel. This represents an equilibrium position in performance. For this situation to be stable, slight perturbations away from exactly equal positive or negative torques must not greatly affect the overall forces experienced by the blades. Contrarily, if the situation is unstable, a slight shift should cause the turbine to either spin down or begin accelerating once more—a situation which matches the "nonself-starting" problem or the behavior of the Durham turbine after the initial velocity plateau.

Such behavior is consistent with the shifting of a flow separation point and the transition from laminar to turbulent flow, which is directly related to the onset and rate of vortex shedding. It is known from theory that during every rotation, each blade cycles through high and low angles of attack, which are associated, respectively, with separated and attached flow (Fig. 12). The blade thus experiences friction drag, significant pressure drag during the former and induced drag during the latter. The friction drag increases as the velocity increases; the induced drag varies inversely, and decreases with increasing velocity. This is complicated by the fact that a turbulent boundary layer also forms as velocity increases, which delays separation and therefore reduces pressure drag [25]. Applying all of this to the turbine, then, the blades should experience the following:

At rest, inertia resists rotation. The blades begin to move due to the pressure applied to them by the wind, and viscous forces act between the fluid and blade surfaces. As an individual blade travels, it generates relatively high lift at a moderate angle of attack, also shedding tip vortices with associated drag. Beyond the stall angle, these tip vortices die off, but flow separation results in a swirling region and large pressure drop behind the tail. The wind continues to apply pressure to each blade, and this combined with the generated lift force results in an acceleration of the turbine. As the turbine spins more rapidly, the induced drag decreases but the friction drag increases. The wakes left by the preceding blades begin to impact the following ones; the blades also continue to

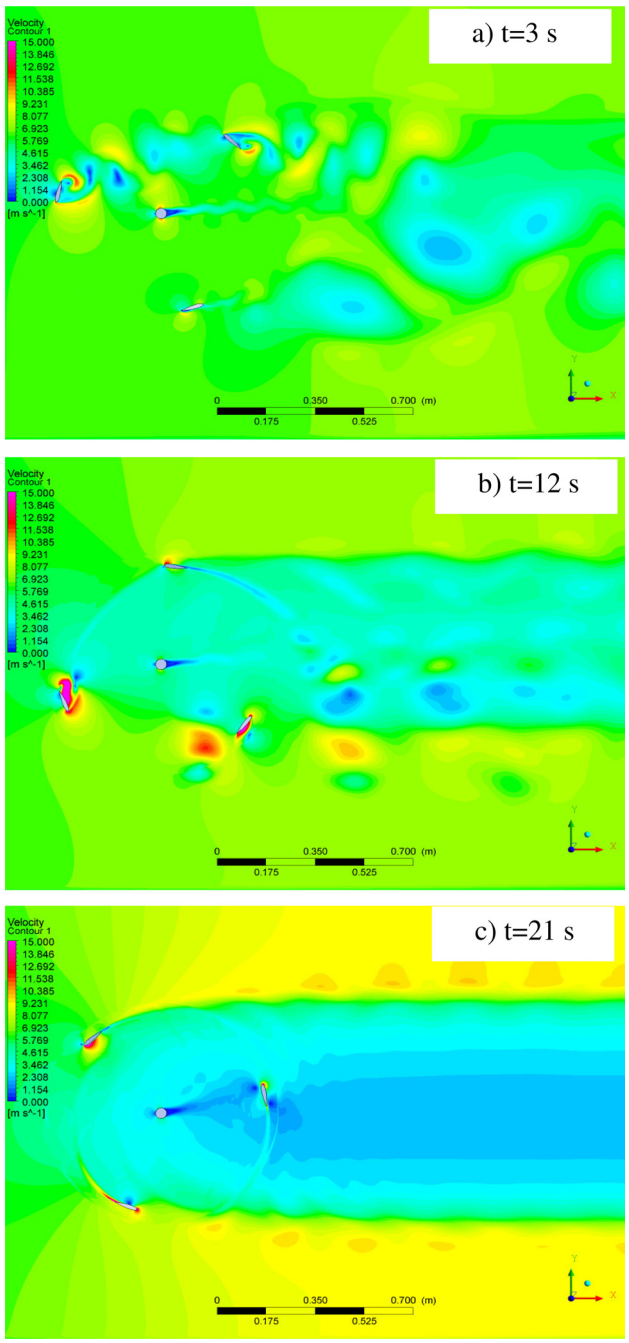

Fig. 13 Medium k-ε turbulence model, velocity contours (m/s) at various times

cycle between low and high angles of attack. As the blade speed approaches the incoming wind speed, the "push" of the wind ceases to drive the turbine at several positions in the cycle. At these positions, the lift force is left to counter the various components of drag discussed, and a dynamic equilibrium between the two is reached. A great deal of turbulence is generated in the domain due to the aforementioned vortex shedding. Moreover, each of the three blades continues to experience a range of apparent winds, with the maximum wind increasing due to entrainment by the blades (Fig. 12). The combination triggers an increasingly early transition from laminar to turbulent boundary layer, with an associated decrease in pressure drag. This decrease in a negative torque results in a net positive, and the turbine again begins to accelerate. As the turbine accelerates, the blades begin to move quickly enough that they present an effective blockage, and the

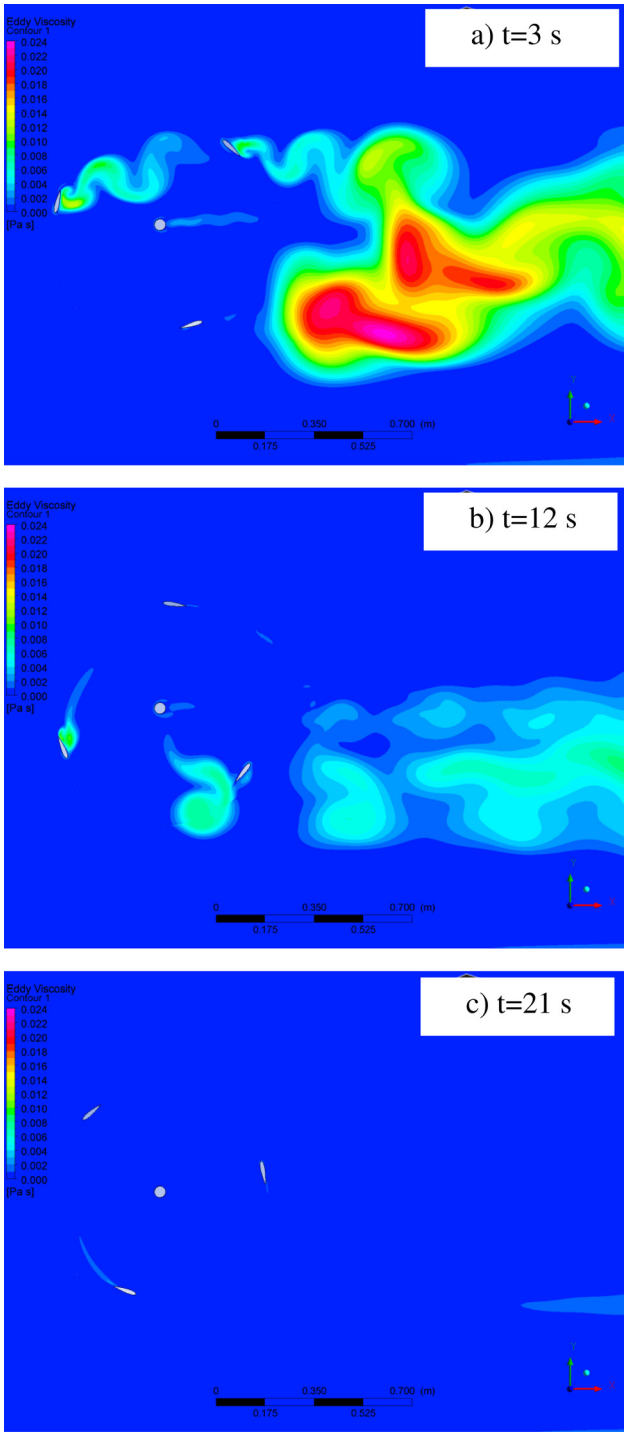

Fig. 14 Medium k-ε Turbulence model, eddy viscosity contours at various times

turbine appears more like a rotating solid cylinder than a fan. Shed vortices are swept outside the turbine region rather than meandering through it, and a new equilibrium position is reached representing the balance of effective solid cylinder lift and drag. Unlike the initial plateau, this one is stable, and thus the turbine maintains a steady operating speed while the incoming wind is constant.

Based on the above reasoning, it is therefore proposed that a good transitional model applied to the 2D simulation should rectify the missing initial velocity plateau, and might better capture the tip vortex effects in 3D [26]. This accuracy of simulation is both desirable and problematic. On the one hand, ability to model the initial plateau allows for insight into potential start-up issues, as well as their causes and solutions. Inclusion of separation phenomena also increases the simulation time tenfold, and with it real computational time. Since tip vortices were not of particular interest in this case and the 3D simulation was excessively time-consuming for no marked gain, all following discussion is strictly 2D.

5.1 Flow Visualization. Some support for the above hypothesis may be gained by examining flow visualization at different times in the turbine ramp-up. Figure 13 shows a contour plot of velocity at a number of timesteps.

Even with the medium k-ε turbulence model, it can be seen that shed vortices from the blades do move downstream, resulting in stagnant regions which slowly advect away or encounter the next blade. As the turbine ramps up to operating speed, these vortices cease to propagate through the wake region; instead, the turbine does begin to look more like a solid rotating cylinder, with a stationary wake and von Karman vortex street whose width is equal to that of the turbine diameter.

This shift in behavior is also reflected in a contour plot of eddy viscosity (Fig. 14). It can be seen that regions of high eddy viscosity initially develop behind the blades, but after a certain time, these die off and are not replaced. The transition occurs exactly where one would expect to see the initial velocity plateau, between about 9 and 15 s. Taking into account the time scaling factor of 10x, this does indeed correspond to the plateau region reported experimentally.

6 Conclusion

A scalable k-ε turbulence model transient CFD simulation has been demonstrated to accurately predict VAWT operating speed within 12% error using a two-dimensional structured mesh in conjunction with a carefully specified series of boundary conditions. It is therefore recommended that this method be used for further parametric studies with the caveat that intermediate turbine performance will not be accurately captured.

In the event that this regime is important, for example in the study of self-starting problems, a blended turbulence model utilizing a k-ω formulation near the walls is recommended. Furthermore, as the separation point appears to affect the performance outcome significantly, a transitional turbulence model should be enabled [27].

Regardless of which turbulence model is chosen, it can further be asserted that little is gained by switching to a three dimensional approach. Such a model often necessitates a poorer mesh quality and needlessly increases computational time. Although tip vortices may be illustrated with this technique, they impact most turbines only modestly, unless the height-to-width ratio is significantly less than 1, a proportion not recommended from an efficiency standpoint anyway. Thus, it is concluded that the choice of fluid dynamics models impacts the simulation outcome far more than the simplification to two dimensions.

Incorporating the discussed recommendations, CFD can become a valuable tool for the design and optimization of vertical axis wind turbines. For example, setting up an optimization problem with design variable related to blade orientation or geometry and solving it using optimization algorithms [28] may lead to optimal designs of vertical axis wind turbines.

Clearly the problems and limitations of VAWTs outlined herein are not unique or insurmountable; they are the same effects encountered by all aerodynamic machines. By applying detailed and accurate computer modeling, such effects may be examined in depth without the expense of large wind tunnels, costly prototypes or complex measurement tools. In doing so, the undeserved poor reputation VAWTs have acquired can be addressed with solid, systematic research and design, and the many benefits of the vertical axis configuration can be realized.

Acknowledgment

The authors would like to thank the members of ROMAC Jefferson Wind Energy group of University of Virginia for helpful feedback and suggestions.

Nomenclature

C = blade airfoil chord, m
c_p = coefficient of performance
R = radial distance, m
S = blade span, m
T = timestep, s
$x, y_{\text{subdomain}}$ = cartesian coordinates of a subdomain node, m
$\dot{x}, \dot{y}_{\text{subdomain}}$ = subdomain velocity components
J = total moment of Inertia, kg $\times$ m^2
J_{eff} = moment of inertia per unit height, kg $\times$ m^2
R = effective swept turbine radius, m
T_z = torque
TSR = V/U tip-speed ratio
U = incoming wind velocity, m/s
V = tangential velocity due to turbine rotation, m/s
W = apparent wind velocity, m/s
θ = blade azimuth angle (position)
$\dot{\theta}$ = angular velocity
$\ddot{\theta}$ = angular acceleration

Superscript

n = new

References

[1] Hill, D. R., 1984, *A History of Engineering in Classical and Medieval Times*, Open Court Publishing, La Salle, IL, pp. 173.
[2] Hau, E., 2006, *Wind Turbines: Fundamentals, Technologies, Application, Economics*, Springer-Verlag, Berlin, GER.
[3] Darrieus, G. J. M., 1931, Turbine Having Its Rotating Shaft Transverse to the Flow of the Current, U. S. Patent No. 1835018.
[4] Kirke, B. K., 1998, "Evaluation of self-starting vertical axis wind turbines for stand-alone applications," Ph. D. thesis, Griffith University, Australia.
[5] Colson and Associates, 1995, "Avian Interaction With Wind Facilities: A Summary," American Wind Energy Association.
[6] Pasqualetti, M., 2004, *History of Wind Energy*, Elsevier, Burlington, MA.
[7] Blackwell, B. F., and Reis, G. E., 1974, "Blade Shape for a Troposkien Type of Vertical-Axis Wind Turbine", SLA-74-0154, Sandia National Laboratories, Albuquerque, NM.
[8] *Vertical Axis Wind Turbine: The History of the DOE Program*, VAWT Archives. Sandia National Laboratories, Albuquerque, NM. Available at http://windpower.sandia.gov/topical.htm. Accessed: July 20, 2011.
[9] Baker, J. R., 1983, "Features to Aid or Enable Self-Starting of Fixed Pitch Low Solidity Vertical Axis Wind Turbines," J. Wind. Eng. Ind. Aerodyn., **15**, pp. 369–380.
[10] Sorensen, N. N., Michelsen, J. A., and Schreck, S., 2002, "Navier-Stokes Predictions of the NREL Phase VI Rotor in the NASA Ames 80ftx120ft Wind Tunnel," Wind Energy, **5**, pp. 151–169.
[11] Le Pape, A., and Lecanu, J., 2004, "3D Navier-Stokes Computations of a Stall-Regulated Wind Turbine," Wind Energy, **7**, pp. 309–324.
[12] Tongchitpakdee, C., Benjanirat, S., and Sankar, L. N., 2005, "Numerical Simulations of the Aerodynamics of Horizontal Axis Wind Turbines under Yawed Flow Conditions," ASME J. Sol. Energy Eng., **127**(4), pp. 464–475.
[13] Sezer-Uzol, N., and Long, L. N., 2006, "3-D Time-Accurate CFD Simulations of Wind Turbine Rotor Flow Fields", AIAA Paper No. 2006-0394.
[14] Brahimi, M. T., Allet, A., and Paraschivoiu, I., 1995, "Aerodynamic Analysis Models for Vertical-Axis Wind Turbines," Int. J. Rotating Mach., **2**(1), pp. 15–21.
[15] Paraschivoiu, I., 2002, *Wind Turbine Design: with Emphasis on Darrieus Concept*, Polytechnic International Press, Montreal, CN.
[16] Read, S., and Sharpe, D. J., 1980, *An Extended Multiple Streamtube Theory for Vertical Axis Wind Turbines*, Cranfield, UK, pp. 65–72.
[17] Strickland, J. H., 1976, *A Performance Prediction Model for the Darrieus Turbine*, Cambridge, UK, pp. C3–39–54.
[18] Templin, R. J., 1974, *Aerodynamic performance theory for the NRC Vertical-axis wind turbine*, National Research Council, Canada, p. 29.
[19] Islam, M., Ting, D., and Fartaj, A., 2008, "Aerodynamic Models for Darrieus-Type Straight-Bladed Vertical Axis Wind Turbines," Renewable Sustainable Energy Rev., **12**, pp. 1087–1109.
[20] Betz, A., 1966, *Introduction to the Theory of Flow Machines*, Pergamon, New York, Oxford.
[21] Hill, N., Dominy, R., Ingram, G., and Dominy, J., 2008, "Darrieus Turbines: The Physics of Self-Starting," Proc. Inst. Mech. Eng., Part A, **223**, pp. 21–29.
[22] Howell, R., Qin, N., Edwards, J., and Durrani, N., 2009, "Wind Tunnel and Numerical Study of a Small Vertical Axis Wind Turbine," Renewable Energy, **35**, pp. 412–422.
[23] Ferreira, C. S., van Kuik, G., van Bussel, G., and Scarano, F., 2009, "Visualization by PIV of Dynamic Stall on a Vertical Axis Wind Turbine," Exp. Fluids, **46**(1), pp. 97–108.
[24] Bardina, J. E., Huang, P. G., Coakley, T. J., 1997, "Turbulence Modeling Validation, Testing, and Development," NASA Technical Memorandum 110446.
[25] Batchelor, G. K., 1967, *An Introduction to Fluid Dynamics*, Cambridge University, New York, p. 147.
[26] Menter, F. R., 1994, "Two-Equation Eddy-Viscosity Turbulence Models for Engineering Applications," AIAA J., **32**(8), pp.1598–1605.
[27] Langtry, R. B., Gola, J., Menter, F. R., 2006, "Predicting 2D Airfoil and 3D Wind Turbine Rotor Performance Using Transition Model for General CFD Codes," AIAA Paper No. 2006-0395.
[28] Untaroiu, C., and Untaroiu, A., 2010, "Constrained Design Optimization of Rotor-Tilting Pad Bearings Systems," ASME J. Eng. Gas Turbines Power, **132**(12), pp. 122502.